

# Examination of chemical elements partitioning between the $\gamma$ and $\gamma'$ phases in CMSX-4 superalloy using EDS microanalysis and electron tomography

Adam Kruk, Beata Dubiel<sup>a</sup>, and Aleksandra Czyska-Filemonowicz

AGH University of Science and Technology, International Centre of Electron Microscopy for Materials Science, Faculty of Metals Engineering and Industrial Computer Science, Al. A. Mickiewicza 30, 30-059 Kraków, Poland

**Abstract.** In the present study, the partition of chemical elements between  $\gamma$  and  $\gamma'$  phases in CMSX-4 was investigated using EDS microanalysis and electron tomography (FIB-SEM and STEM-EDS) methods. The investigation has been performed for the superalloy after standard heat treatment and the ex-service CMSX-4 turbine blade after operation for 12 700 hours and 200 starts in industrial gas turbine. The results have shown that Co, Cr and Re partition to the  $\gamma$  matrix, Ni and W are present in both  $\gamma$  and  $\gamma'$  phases, while Al, Ti and Ta strongly partition to the  $\gamma'$  phase. The results show the abilities of new analytical electron microscopy and electron tomography methods to characterize the microstructure and chemical composition of single crystal superalloys at the nanoscale.

## 1. Introduction

The single crystal nickel-base CMSX-4 superalloy is widely used for gas turbine blades. Its microstructure is especially tailored to ensure high microstructure stability and high temperature strength by the absence of grain boundaries, strengthening by high volume fraction of cuboidal intermetallic  $\gamma'$  precipitates and nanometric width of  $\gamma$  matrix channels. Although the partitioning of chemical elements between  $\gamma$  and  $\gamma'$  phases in single crystal superalloys is known from literature, this knowledge is based mainly on the results obtained by means of X-ray spectroscopy methods with wavelength dispersion (WDS) [1, 2] and energy dispersion (EDS) with Si-Li detectors [e.g. 3–5].

The spatial resolution of WDS is about 100 nm, what means that this method is not appropriate for determination of chemical composition in  $\gamma$  phase channels, because their width in single crystal superalloys is in the range 30–90 nm. Therefore, the WDS microanalysis is rather appropriate for the analysis of segregation of chemical elements between dendritic and interdendritic regions.

Much better spatial resolution of microanalysis can be obtained with use of conventional analytical electron microscope with field emission gun and Si-Li EDS detector, both in transmission (TEM) and scanning transmission (STEM) electron microscopy mode, due to the possibility to converge the electron beam down to about 1 nm diameter. However, the small take-off angle about 0.3 sr and the limited count number at such a small beam diameter and beam current are the main factors

influencing the relatively low accuracy of the quantitative EDS microanalysis.

In the recent years pronounced development was achieved in instrumentation and methodology of analytical electron microscopy. Application of high brightness field emission (X-FEG) electron sources, correction of spherical aberration (Cs) of condenser lenses and increase of the efficiency of EDS microanalysis by combination of four silicon drift detectors (SDD) in ChemiSTEM<sup>TM</sup> system allows to perform high spatial resolution chemical microanalysis even below 0.1 nm, using various methods of point analysis, one-dimensional line profiles, two-dimensional elemental maps or three dimensional STEM-EDS electron tomograms.

Application of electron tomography methods, both (S)TEM-EDX and Focused Ion Beam Scanning Electron Microscopy (FIB-SEM) tomography, is especially advantageous because it gives the possibility to reconstruct both the microstructure and chemical composition in three dimensions.

In the present paper, the results of the examination of the morphology and chemical composition of  $\gamma$  and  $\gamma'$  phases in single crystal CMSX-4 superalloy after standard heat treatment as well as in the ex-service turbine blade using new analytical electron-microscopy and tomography techniques mentioned above are presented.

## 2. Material and experimental methods

The investigation was performed using CMSX-4 single crystal nickel-base superalloy in the form of heat treated solid bars and ex-service gas turbine blade. The nominal

<sup>a</sup> Corresponding author: [bdubiel@agh.edu.pl](mailto:bdubiel@agh.edu.pl)

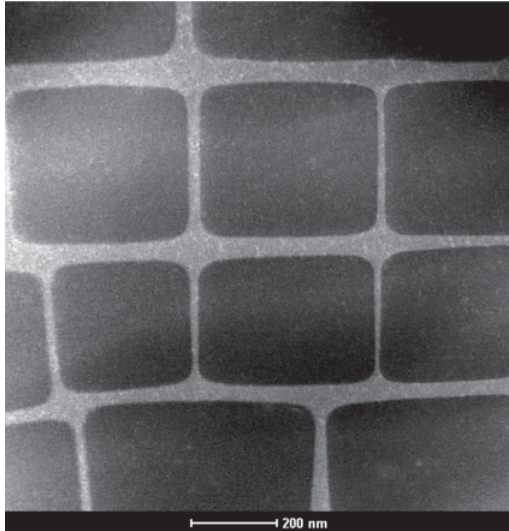


**Figure 1.** STEM-HAADF image showing the cuboidal morphology of  $\gamma'$  particles in the as-received CMSX-4. The brighter contrast of  $\gamma$  phase channels corresponds to larger Z-number of the chemical elements partitioning to  $\gamma$  channels.

chemical composition of CMSX-4 was the following (wt%): Ni – 8.4 Co – 6.4 Cr – 6.5 Ta – 6.4 W – 5.68 Al – 2.8 Re – 1.04 Ti – 0.58 Mo. Heat treated (001) solid bars were kindly supplied by Howmet Ltd, UK. The ex-service blade was supplied by SIEMENS Industrial Turbomachinery Ltd, Lincoln after operation for 12 700 hours in the stationary gas turbine. According to SIEMENS specification, the distribution of temperature and stress in the blade was as follows: 997 °C/ 30 MPa at the blade tip, 927 °C/111 MPa at the middle of the blade height and 807 °C/189 MPa at the blade bottom.

Microstructural analyses were carried out by means of electron microscopy (STEM, STEM-EDS) using a probe Cs corrected Titan<sup>3</sup> G2 60–300 electron microscope equipped with a ChemiSTEM™ system of FEI. The site specific specimens (lamellas) for STEM investigation were prepared utilizing a NEON CrossBeam 40EsB microscope of Zeiss. This microscope was also used for FIB-SEM tomography.

STEM analyses were performed using high angle annular dark-field (HAADF) mode. The EDS microanalysis with ChemiSTEM™ detection system of the FEI allowed to acquire high X-ray signal elemental maps over a large tilt angle of the sample and collect a tomographic series of 2D STEM-EDS maps in the angular range from  $-40^\circ$  to  $+60^\circ$  with step of  $5^\circ$ . Tomographic reconstruction of a tilt series of STEM-EDS maps was performed using ART method [6], which allowed visualizing the three-dimensional distribution of chemical elements in the analysed volume. FIB-SEM tomography was carried out using a serial slicing technique. Serial FIB cross-sections in-situ milling was performed by Ga-ion beam at 30 kV through the investigated volume and each exposed surface was imaged with the BSE detector. The distance between slices was about 8 nm. Consequently, the acquired stack of images was transformed directly into a 3D data volume with a voxel resolution of  $8 \times 8 \times 8$  nm. The experimental details of FIB-SEM tomography are given elsewhere [7].

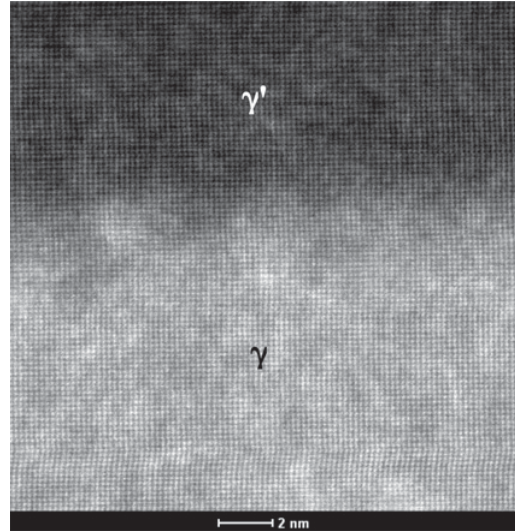


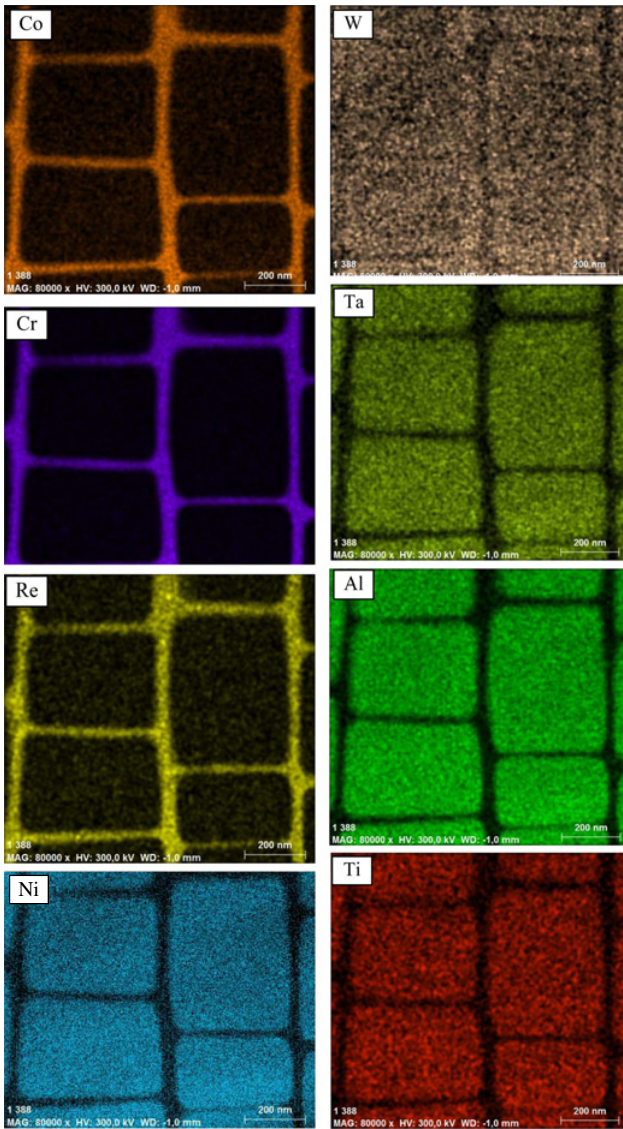
**Figure 2.** High resolution STEM-HAADF image of  $\gamma$ - $\gamma'$  interface in the as-received CMSX-4 superalloy.

### 3. Results and discussion

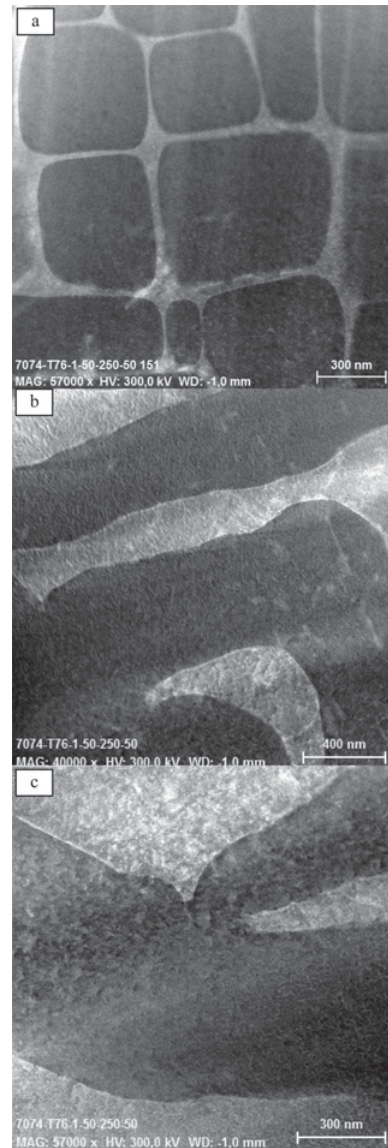
The microstructure of CMSX-4 superalloy consists of cuboidal precipitates of  $\gamma'$  phase ( $\text{Ni}_3\text{Al}$  – based), coherent with  $\gamma$  solid solution matrix. Figure 1 shows the medium resolution STEM-HAADF image of CMSX-4 microstructure after standard heat treatment, viewed along [001] zone axis. Since the contrast is approximately proportional to  $Z^2$  ( $Z$ : atomic number),  $\gamma$  matrix channels with higher mean atomic number are seen as brighter than precipitates of  $\gamma'$  phase, containing lighter elements. The high resolution STEM-HAADF image of  $\gamma$ - $\gamma'$  interface is shown in Fig. 2. The brighter dots in  $\gamma$  phase correspond to the atomic columns containing heavier atoms.

Figure 3 shows the STEM-EDS chemical mapping of as-received CMSX-4 superalloy. It can be seen that Co, Cr and Re partition to the  $\gamma$  phase. The content of Ni and W in  $\gamma$  matrix is smaller than in  $\gamma'$  precipitates, which contains also Ta, Al and Ti. Temperature-dependent partitioning of chemical elements between  $\gamma$  and  $\gamma'$  phases is one of the factors influencing the changes in morphology of  $\gamma'$  particles in single crystal superalloys under long-term high temperature and stress exposure.

Microstructural analyses of the turbine blade after service in the stationary gas turbine carried out by means of FIB-SEM tomography (Fig. 4) and STEM-HAADF (Fig. 5) revealed the pronounced differences in  $\gamma'$  phase morphology in different parts of the airfoil. At the bottom of the blade (the lowest temperature of 807 °C and the highest applied stress of 189 MPa), the cuboidal morphology of  $\gamma'$  precipitates was preserved and the microstructure was similar to the as-received material. The microstructural changes of the CMSX-4 blade during service were more distinct in the middle and the top, both at the leading and trailing edge. In the middle of the blade height (temperature of 927 °C and stress of 111 MPa), the well-developed rafts oriented perpendicularly to the longitudinal axis of the airfoil were observed. At the top of the blade (the highest temperature of 997 °C, the lowest applied stress of 30 MPa) and the microstructure was



**Figure 3.** STEM-EDS elemental maps of  $\gamma$  and  $\gamma'$  phases in CMSX-4 superalloy subjected to standard heat treatment.



**Figure 5.** STEM-HAADF images of the microstructure at the a) bottom, b) middle of the height and c) top of the ex-service turbine blade.

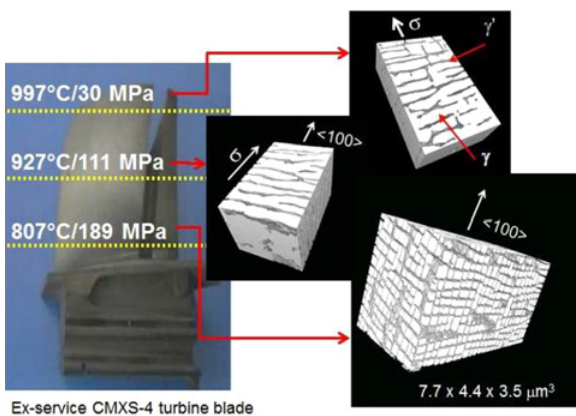


**Figure 4.** 3D visualization of  $\gamma$  and  $\gamma'$  phases in reconstructed volume  $7.7 \times 4.4 \times 3.5 \mu\text{m}^3$  in the ex-service turbine blade, FIB-SEM tomography.

characterized by wavy  $\gamma$ - $\gamma'$  rafts, thicker and shorter than in the blade middle zone. The more detailed description of the microstructure evolution in the exservice turbine blade is given in Ref. [8]. It is well established that the change of the  $\gamma'$  particles shape from cubes to plates during rafting proceeds by diffusion of  $\gamma$ -partitioning elements out of the vertical channels and  $\gamma'$ -partitioning elements into them. STEM-EDS elemental maps revealed the chemical composition of  $\gamma$  and  $\gamma'$  rafts (Fig. 6) in the middle of the blade. The wavy shape of  $\gamma$ - $\gamma'$  interfaces is related with their diffusion induced migration.

The other method used for 3D imaging of the microstructure and chemical composition in the middle zone of the CMSX-4 turbine blade was STEM-EDS tomography. STEM-HAADF images and the corresponding STEM-EDS maps of chromium acquired at

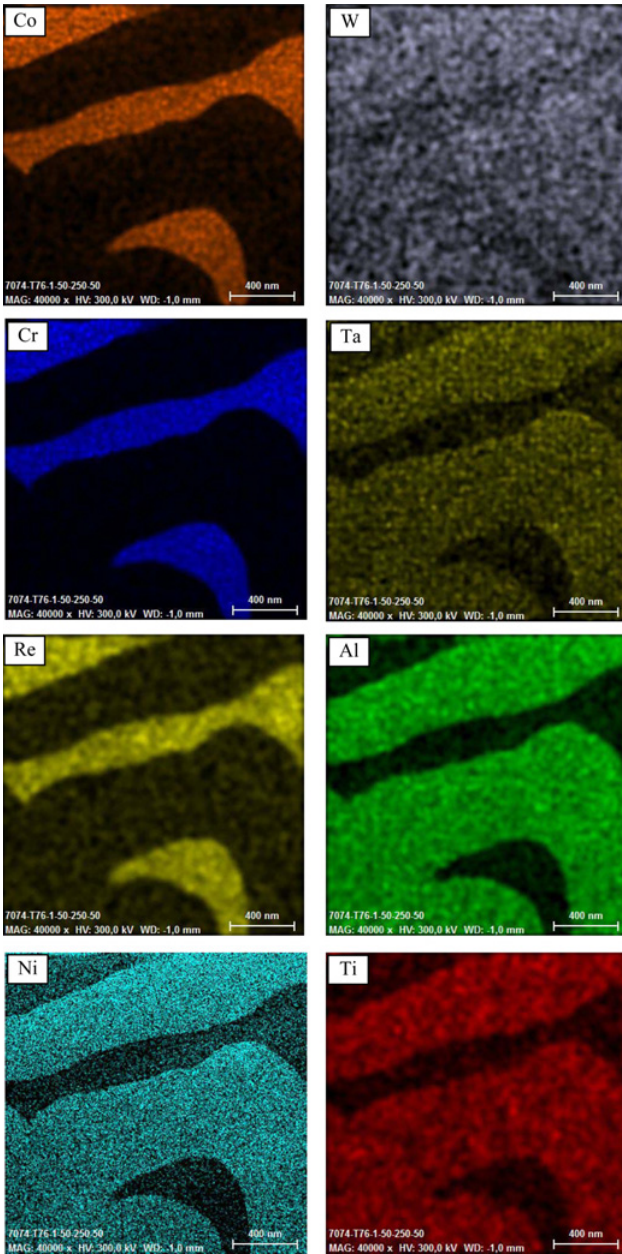


**Figure 6.** STEM-EDS elemental maps of  $\gamma$  and  $\gamma'$  phases in the middle zone of the ex-service CMSX-4 gas turbine blade.

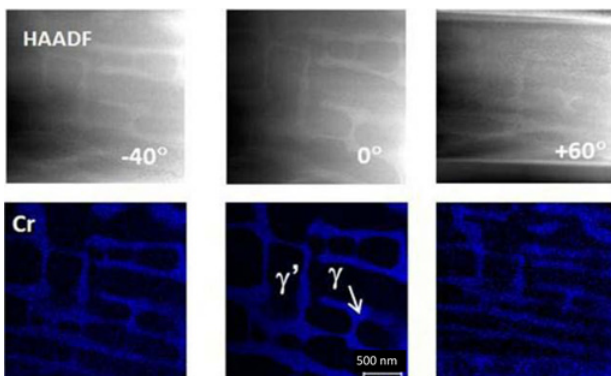


**Figure 7.** STEM-HAADF images and STEM-EDS Cr maps at  $-40^\circ$ ,  $0^\circ$  and  $60^\circ$  tilt angle, selected from the registered tilt series.

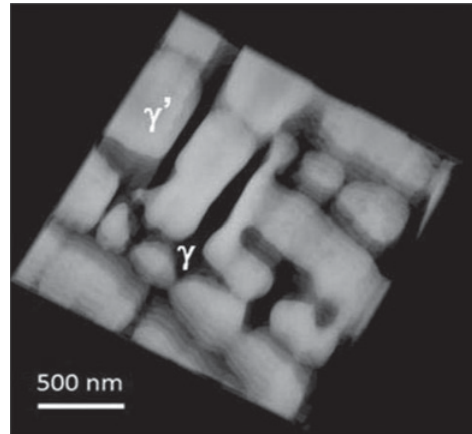


**Figure 8.** 3D visualization of  $\gamma$  and  $\gamma'$  phases in reconstructed volume of  $7.7 \times 4.4 \times 3.5 \mu\text{m}^3$  in the ex-service turbine blade, STEM-HAADF.

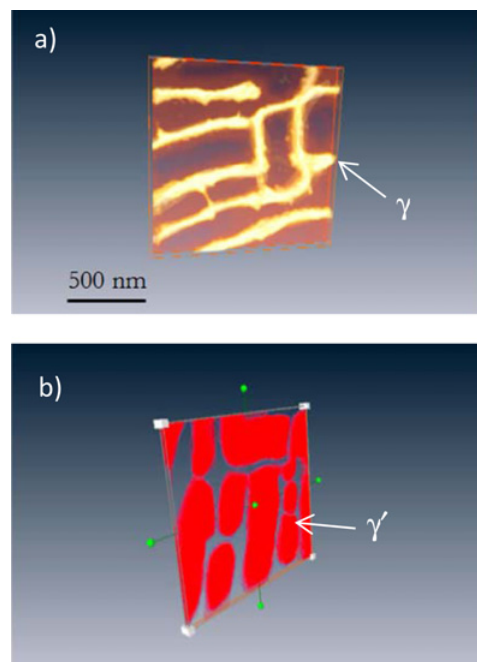


**Figure 9.** 3D visualization of reconstructed volume of the ex-service turbine blade, a) visualization of  $\gamma$  phase channels (based on STEM-EDS Cr maps), b) visualization of  $\gamma'$  phase (based on STEM-EDS Al maps).

$-40^\circ$ ,  $0^\circ$  and  $60^\circ$  tilt angle, selected from the registered tilt series, are shown in Fig. 7. As chromium partitions to the  $\gamma$  phase, its distribution illustrates indirectly the morphology of  $\gamma$  channels. 3D visualization of  $\gamma$  and  $\gamma'$  phases is presented in Figs. 8 and 9. It can be observed that the rafts are rather short and the remaining vertical  $\gamma$  channels are present.

#### 4. Summary

The microstructure and chemical composition of  $\gamma$  and  $\gamma'$  phases in the CMSX-4 superalloy after standard heat treatment as well as long-term exposure of the blade in the stationary gas turbine was investigated by means of

several new analytical electron microscopy and electron tomography methods.

It was observed that Co, Cr and Re have a relatively high solubility in  $\gamma$  matrix, while Ni and W are present in both  $\gamma$  and  $\gamma'$  phases. Al, Ti and Ta strongly partition to the  $\gamma'$  phase.

Investigation of the turbine blade has shown that its microstructure is unstable during service. The observed diversification of the  $\gamma'$  morphology along the blade height is caused by the differences in temperature and stress acting. 2D STEM-EDS elemental maps and 3D STEM-EDS tomography revealed the distribution of chemical elements in the middle of the blade with rafted  $\gamma$ - $\gamma'$  microstructure.

The presented results illustrate new possibilities of microstructure and chemical composition characterisation of single crystal superalloys taking advantage of recent development in analytical electron microscopy and electron tomography.

The financial support by the European Union under the Framework 7 Program contract for an Integrated Infrastructure Initiative, reference 312483 ESTEEM2 is gratefully acknowledged. The authors thank Howmet, Exeter, UK, for providing the CMSX-4 material and SIEMENS Industrial Turbomachinery

Ltd, Lincoln, UK, for the ex-service blade provided within COST Action 538, as well as Mr A. Gruszczyński, MSc., K. Płońska-Niżnik (AGH-UST) and Dr A. Carlsson (FEI) for their assistance in the investigation.

## References

- [1] R.M. Kearsey, J.C. Beddoes, P. Jones, P. Au, *Intermetallics* **12**, 903 (2004)
- [2] R.C. Reed, D.C. Cox, C.M.F. Rae, *Mater. Sci. Tech.* **23**, 893 (2007)
- [3] E.C. Caldwell, F.J. Fela, G.E. Fuchs, *Superalloys 2004* (The Minerals, Metals & Materials Society, Warrendale PA 2004)
- [4] A.I. Epishin, I.L. Svetlov, N.V. Petrushin, Y.V. Loshchinin, T. Link, *Defect Diffus. Forum* **309-310**, 121 (2011)
- [5] F. Sun, J. Zhang, P. Liu, Q. Feng, X. Han, S. Maob, J. *Alloys Compd.* **536**, 80 (2012)
- [6] R. Gordon, R. Bender, G.T. Herman, *J. Theor. Biol.* **29**, 471 (1970)
- [7] A. Kruk, A. Czyska-Filemonowicz, *Arch. Metall. Mater.* **58**, 387 (2013)
- [8] B. Dubiel, A. Czyska-Filemonowicz, *Solid State Phenom.* **186**, 139 (2012)